DOI: http://dx.doi.org/10.12989/sem.2008.28.4.387

Fatigue life prediction of horizontally curved thin walled box girder steel bridges

K. Nallasivam†, Sudip Talukdar‡ and Anjan Dutta‡†

Department of Civil Engineering, Indian Institute of Technology Guwahati-781039, India

(Received August 8, 2006, Accepted January 7, 2008)

Abstract. The fatigue damage accumulation rates of horizontally curved thin walled box-girder bridge have been estimated from vehicle-induced dynamic stress history using rain flow cycle counting method in the time domain approach. The curved box-girder bridge has been numerically modeled using computationally efficient thin walled box-beam finite elements, which take into account the important structural actions like torsional warping, distortion and distortional warping in addition to the conventional displacement and rotational degrees of freedom. Vehicle model includes heave-pitch-roll degrees of freedom with longitudinal and transverse input to the wheels. The bridge deck unevenness, which is taken as inputs to the vehicle wheels, has been assumed to be a realization of homogeneous random process specified by a power spectral density (PSD) function. The linear damage accumulation theory has been applied to calculate fatigue life. The fatigue life estimated by cycle counting method in time domain has been compared with those found by estimating the PSD of response in frequency domain. The frequency domain method uses an analytical expression involving spectral moment characteristics of stress process. The effects of some of the important parameters on fatigue life of the curved box bridge have been studied.

Keywords: fatigue life; horizontally curved; thin walled box-girder; finite elements; cycle counting; linear damage accumulation; power spectral density.

1. Introduction

The use of horizontally curved thin-walled box girder bridges has substantially increased in the recent past due to various reasons, such as the need for smooth dissemination of congested traffic, limitation of right of way, aesthetic, economic and environmental considerations. The passage of vehicles over the bridge induces its self weight in addition to dynamic tyre force resulted from the vibration of vehicles due to unevenness of the deck. The horizontally curved thin walled section bridge girders present more complicated structural action, where bending and torsion due to moving loads are coupled resulting in transverse and lateral deformation accompanied by warping as well as distortion of girder cross section. Unlike straight bridges, the horizontally curved bridges are additionally loaded due to centrifugal thrust, which are liable to affect the dynamic characteristics of the bridge.

† E-mail: nallasivam@iitg.ernet.in
‡ Associate Professor, Corresponding author, E-mail: staluk@iitg.ernet.in
‡† E-mail: adutta@iitg.ernet.in

Fatigue is an important consideration for the design of bridges due to repeated action of moving loads Fatigue behaviour of structures has been studied by several authors theoretically as well as experimentally. Bennantine *et al.* (1990) described the theory of fatigue damage in metallic specimens. It is customary to study fatigue strength of the structural member based on constant amplitude fatigue test. The constant amplitude fatigue test result is usually represented in the form of S-N curve (S: stress range, N: number of cycles to failure). Miner (1945) used S-N curve approach to formulate a linear damage accumulation rule enabling one to predict fatigue damage at each incremental stress range. Fatigue design criteria based on the S-N curve approach in conjunction with linear damage hypothesis has been incorporated in American Association of State Highway and Transportation Official's (AASHTO) guide specification for fatigue of steel bridges (1989), in British Standard Institution's code of practice for fatigue design of steel, concrete and composite bridges (1980), in Indian Railway's bridge rules (1964) and in Indian Road Congress (IRC) specification for road bridges of composite construction (1986). The drawback of these methods lies on the fact that the charts used are based on constant amplitude fatigue test data, which does not reflect the stress developed in the members due to the dynamic interaction of vehicles with the bridge.

When structures or components are subjected to repeated applications of random forces, as with traffic loadings on the bridge, the number of cycles at which failure occurs are random variables. Dowling (1972) developed statistical cycle counting method for handling the complicated stress cycles induced by the variable amplitude load. Wirsching and Light (1980) conducted a study to develop an engineering model which was used for design purposes to predict metal fatigue under wide band random process. Lutes *et al.* (1984) presented a stochastic fatigue damage theory to model uncertainty about stress time history. Numerical simulations were performed based on the existence of S-N curves for constant amplitude fatigue. Larson and Lutes (1991) conducted study on the prediction of fatigue life of off shore structures by spectral density approach. It was applied to unimodal and bi-modal power spectral density function with the use of only single moment integral. Such an approach was found useful when one would need to predict fatigue life without knowing all the details of loading and stress time history.

An alternative way for the fatigue assessment study of the structural members has been based on the principles of fracture mechanics, which assumes an initial crack of a certain length and envisages its propagation until it has attained a critical length. Paris and Erdogen (1963) developed a crack growth model which formed the basis of such study. The linear fracture mechanics approach was found to be inadequate in predicting fatigue failure of strain hardening material in the presence of plasticity near crack tip Woo *et al.* (2004) developed finite element model to predict the elastic-plastic crack tip field and applied the theory to centre-cracked panels (CCP) with ductile fracture under large scale yielding conditions. From practice, it is generally known that a bridge with a fatigue crack can serve for a long time in normal conditions. Zhao *et al.* (1994) and Ravi and Ranganathan (1994) conducted studies on fatigue reliability of bridge components taking account of the phase of crack propagation. Park *et al.* (2005) developed analytical model to estimate fatigue damage of steel bridge welded member using elastic fracture mechanics approach. Their study concluded that crack opening stress is the primary factor effecting failure time.

Bridge fatigue damage can be estimated using either deterministic approach or probabilistic model. Mohammadi *et al.* (1998) presented the application of field data for condition assessment and prediction of service life of highway bridges composed of steel girders with reinforced concrete deck slabs using probability model. The field data compiled for several bridges was used to develop probability density function of stress range. The probability function so developed has been used along with Miner's rule to determine reliability of the failure of components at fatigue critical locations. Agerskov and Nielsen (1999) studied fatigue damage accumulation in steel highway bridge under random loading, and comparisons among experimental results, results of fracture mechanics analysis, and results obtained using current codes and specifications, i.e., Miner's rule, were presented.

Dougall *et al.* (2006) focused on the fatigue damage caused in steel bridge girders by the dynamic tyre forces that occurred during the crossing of heavy transport vehicles. This work quantified the difference in the fatigue life of a short-span and a medium-span bridge due to successive passages of either a steel-sprung or an air-sprung vehicle. Huang *et al.* (1993) calculated the fatigue lives of highway steel bridges using a reliability-based methodology. The fatigue life of both non-composite and composite steel beam bridges for different vehicle speeds and classes of road surface roughness were calculated from the generated stress time-histories. Wang *et al.* (2000) performed truck loading and fatigue damage analysis for girder bridges based on the weight-in-motion data. Fatigue damage analysis was performed according to the miner's linear damage rule. The studies were conducted based on the hypothesis of fatigue damage accumulation and was well suited for structures in the design phase. Repetto (2005) emphasized the need to establish the bounds of fatigue life as an essential condition in the design of structures and illustrated the approach for the case of a wind induced fatigue.

The fatigue provisions in the current codes of practice for the design of steel bridges do not utilize the stresses induced in the bridge components due to dynamic interaction with the moving vehicles. This is particularly significant in the case of curved thin walled box girder configurations because of coupling of flexural and torsional stresses accompanied by warping and distortion of the cross section. It has been found from the literature survey that studies on fatigue life particularly pertaining to a horizontally curved thin walled box girder bridges have not been addressed. With this in view, an elaborate study has been undertaken to estimate the fatigue life of a curved thin walled box girder bridge from the vehicle induced stress history. The use of both time domain and frequency domain method for the fatigue life evaluation has been illustrated for the problem under investigation. A finite element analysis has been performed for the bridge-vehicle coupled dynamic problem using an element, which is computationally efficient as well as reasonably representative of thin-walled box girder behaviour. In the time domain approach, Rainflow Counting Method (RFCM) as proposed by Amzallag *et al.* (1994) has been applied to dynamic stress history of horizontally curved girder of thin walled box section to find the number of cycles and the corresponding stress range. For each stress range, the fraction of total damage has been calculated using Miner's rule and the cumulative damage index is evaluated. Fatigue life of the bridge deck has been found from the cumulative damages in the critical location. In frequency domain approach, the power spectral density of stress at critical location of the bridge has been found to determine spectral moments. These spectral moments are subsequently used in an analytical expression developed by Kihl *et al.* (1995) for fatigue damage accumulation rates based on the assumption of Raleigh's distribution for the probability density function of peaks. The results of fatigue damage obtained by two methods have been compared. Finally, a parametric study has been conducted to examine the influence of some of the important bridge-vehicle parameters on the fatigue life of the curved bridge.

The fatigue testing of structural specimen being time consuming and expensive affairs, the present method of rapid estimate of the fatigue life of a bridge is very attractive in design phase as well as in service to monitor the structural health for various conditions of truck weight and traffic volume. The approach uses the vehicle induced stress and traffic data to arrive at the estimate of fatigue life. The estimation of fatigue life can be achieved in practice by proper traffic study and compiling resultant stress/strain histories of an instrumented bridge at few critical locations.

2. Bridge-vehicle interaction model

In order to apply the concept of fatigue damage accumulation in a curved box girder bridge, the vehicle-induced stresses at the critical sections have to be found by solving a bridge-vehicle dynamic interaction problem. In the first step, appropriate models for the bridge and vehicle have to be selected for numerical simulation of the coupled dynamics. In the present paper, finite element model has been adopted to simulate the structural actions of a horizontally curved thin walled box girder bridge. The models of bridge and vehicle have been described in the following sections.

2.1 Finite element model of thin walled curved bridge

A three-dimensional finite element analysis offers the most comprehensive treatment, where a variety of structural geometries, supports and loading conditions can be accommodated for the accurate assessment of structural effects. However, such an analysis is highly computational intensive and in some cases leads to voluminous data output. At the preliminary analysis and design stage, it is likely that a three-dimensional analysis may not be very reasonable since the bridge geometries and loading conditions, etc. may have to be modified for diverse reasons. It is, therefore, desirable at this stage to use a realistic, computationally efficient and less expensive model in the analysis.

A three noded one dimensional box beam element has been introduced following the strategy given by Zhang and Lyons (1984) for the coupled bridge-vehicle dynamic analysis. The adopted element is simple, computationally efficient; but very well representative of complex behaviour of thin walled box-girder bridge. Since the element has not been used for dynamic analysis as per the available literature, experimental studies have been conducted by the authors to evaluate the modal parameters (Nallasivam *et al.* 2007), which have matched very well with the numerically evaluated values. The adopted thin-walled box beam element can be regarded as a general beam element. In addition to the usual six degrees of freedom at each node, represented by the three displacements and the three rotations, three more degrees of freedom have been incorporated in the formulation to account for the warping and distortion effects, which occur in box beams. The element is curved in space but the cross-sections are generated by straight lines. The element axis is defined as the locus of the centroids, which may be eccentric from but parallel to the flexural axis. The element has two end nodes and a midpoint node situated on the axis. The three noded thin-walled box beam element is as shown in Fig. 1. A local rectangular coordinates system (x, y, z) along the curve axis is used in the element formulation. The global Cartesian coordinates are in terms of a natural coordinatex, which varies between -1 and $+1$ on the respective faces of the element. The generalized displacements in the local co-ordinate system incorporating all the complexities of a thin-walled box girder are given by

$$\bar{\delta} = [u, v, w, \theta_x, \theta_y, \theta_z, \theta'_x, \gamma_d, \gamma'_d]^T \tag{1}$$

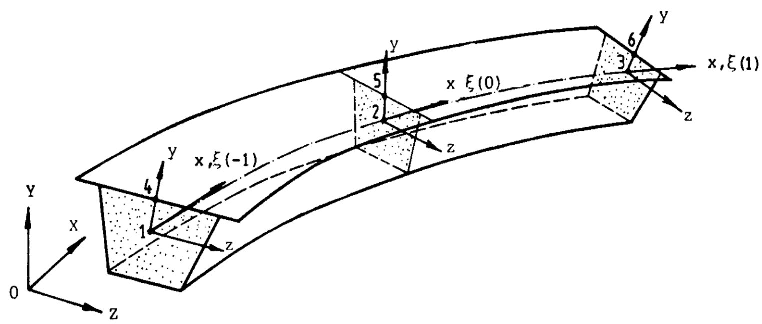

Fig. 1 Curved thin-walled box beam element with three nodes

where u, v, w are the translations along the local x, y, z axes respectively, θ_x is the angle of twist, θ_x' is the rate of twist, θ_y and θ_z are bending rotations about y and z axes respectively, γ_d is the distortion angle, γ_d' is the rate of distortion.

The generalized stress vector is

$$\sigma = \left[N_x, Q_y, Q_z, M_T, M_y, M_z, \frac{1}{\mu_t}B_1, M_d, B_{11}\right]^T \tag{2}$$

in which N_x is the axial force, Q_y, Q_z are the shear forces, M_T is the pure torsional moment, M_y, M_z are the primary bending moments, B_1 is the torsional warping bimoment, M_d is the distortional moment, B_{11} is the distortional warping bimoment and μ_t is the warping shear parameter.

The generalized strain vector is

$$\varepsilon = [\varepsilon_x, \varepsilon_{yx}, \varepsilon_{zx}, \psi_{\theta x}, \psi_{yx}, \psi_{zx}, \psi_{wtx}, \psi_{dx}, \psi_{wdx}]^T \tag{3}$$

where, ε_x represents axial strain in x direction, ε_{yx} and ε_{zx} represent shear strain in y and z direction respectively; $\psi_{\theta x}$, ψ_{yx}, ψ_{zx}, ψ_{wtx}, ψ_{dx}, ψ_{wdx} denote torsional strain, flexural strain in y direction, flexural strain z direction, torsional warping strain, distortional strain and distortional warping strain respectively.

The generalized elasticity matrix [D] required for the calculation of element stiffness and mass matrix is given by

$$[D] = \begin{bmatrix} EA & & & & & & & & \\ & GA_{sy} & & & & & 0 & & \\ & & GA_{sz} & & & & & & \\ & & & GJ_T & & & & & \\ & & & & EI_y & & & & \\ & & & & & EI_z & & & \\ & & & & & & \frac{1}{\mu_t}E_1J_I & & \\ & & 0 & & & & & E_1J_d & \\ & & & & & & & & E_1J_{II} \end{bmatrix} \tag{4}$$

where A is the cross-sectional area; A_{sy}, A_{sz} are effective shear areas in the y and the z directions respectively; J_T is torsional moment of inertia; I_y, I_z are bending moments of inertia about the y and z axes respectively; J_I is torsional warping moment of inertia; J_d is distortional second moment of area; and J_{II} is distortional warping moment of inertia. E_1 is the conversion modulus of elasticity and is given by

$$E_1 = \frac{E}{(1-\nu^2)} \tag{5}$$

where E and ν are the Young's modulus of elasticity and Poisson's ratio. Further, the bending moments of inertia have been calculated on the basis of an effective flange breath replacing the actual width to account for the effect of shear lag. Only C_0 continuity is required for the extensional and flexural effects and quadratic shape functions have been used

$$N_i = \frac{1}{2}(\xi^2 + \xi_0) \quad \text{for } i = 1 \text{ and } 3$$
$$N_i = (1-\xi^2) \quad \text{for } i = 2 \tag{6}$$

However, since the governing equations for torsion and distortion are of fourth order and the beam being three-noded, fifth order C_1 continuity is required for torsion and distortion.

$$N_{i1} = \left(\frac{\xi^2}{4}\right)(4 + 5\xi_0 - 2\xi^2 - 3\xi_0^3) \quad \text{for } i = 1 \text{ and } 3$$
$$N_{i2} = \left(\frac{J_i}{4}\right)\xi^2(1-\xi_0)(1-\xi^2) \tag{7}$$
$$N_{i1} = (1-\xi^2)^2 \quad \text{for } i = 2$$
$$N_{i2} = J_i\xi(1-\xi^2)^2$$

where $\xi_0 = \xi\xi_i$ and J_i is the Jacobian factor with respect to nodal coordinates.

The element stiffness matrix may be written as

$$[k_e] = \int_{-l/2}^{l/2} [B]^T[D][B]dx = \int_{-1}^{+1} J[B]^T[D][B]d\xi \tag{8}$$

where $[B]$ is the strain displacement matrix.

The element mass matrix may be written as

$$[m_e] = A\int_{-l/2}^{l/2} [N]^T\rho[N]dx = A\int_{-1}^{+1} J[N]^T\rho[N]d\xi \tag{9}$$

2.2 Equations of motion for coupled bridge-vehicle system

A rigid vehicle model with heave, pitch and roll degrees of freedom has been considered. The model of vehicle is shown in Fig. 2. Though the vehicle model is a simple two axles one, it is fully

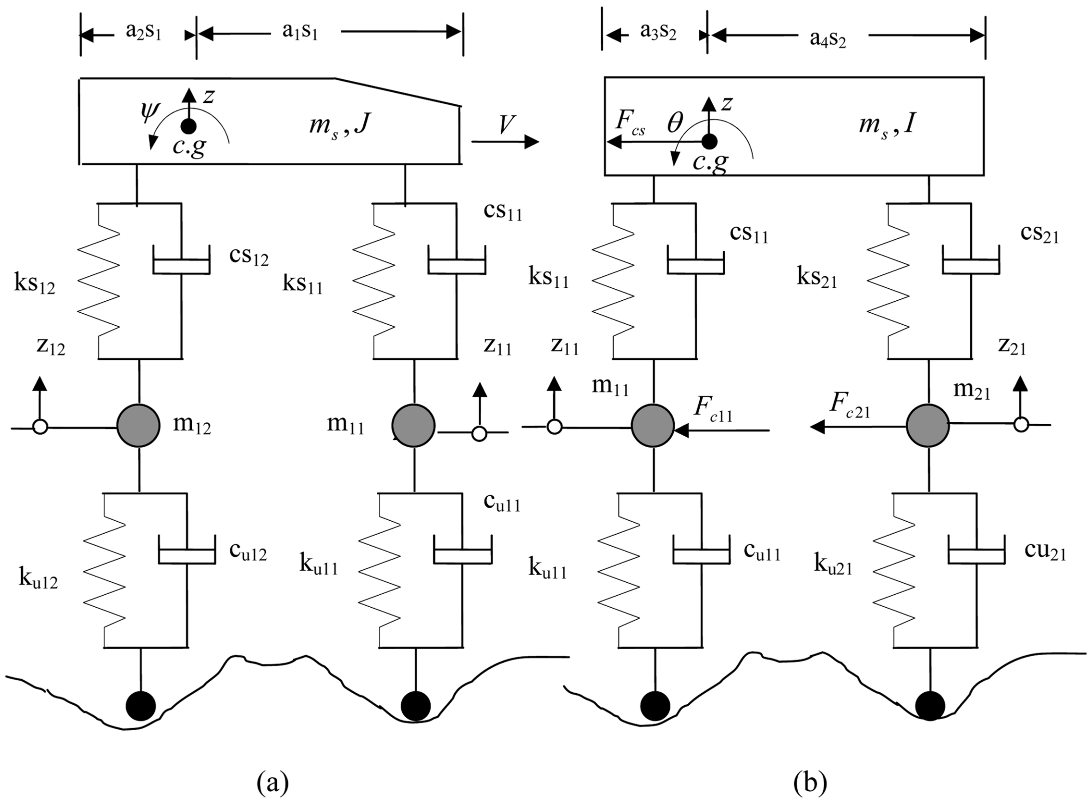

Fig. 2 3-D Vehicle model with seven degrees of freedom (a) Side view (b) End view

capable of idealizing all the important motion components of the vehicle like vertical displacement of the chassis centre (bounce), pitching and rolling rotations about the two axes of the chassis and four vertical displacement of wheel tyres at each of its axle locations and their interaction.

The equation of heave motion of the sprung mass can be written as

$$m_s\ddot{z} + \sum_{i=1}^{2}\sum_{p=1}^{2}\{cs_{ip}(\dot{z} - b_i\dot{\theta} - l_p\dot{\psi} - \dot{z}_{ip}) + ks_{ip}(z - b_i\theta - l_p\psi - z_{ip})\} = 0 \quad (10)$$

As the random input of deck profile is not same for the front and rear wheels, the vehicle is subjected to pitching. The pitching motion of sprung mass is given by

$$J\ddot{\psi} + \sum_{i=1}^{2}\sum_{p=1}^{2}\{-cs_{ip}(\dot{z} - b_i\dot{\theta} - l_p\dot{\psi} - \dot{z}_{ip})l_p - ks_{ip}(z - b_i\theta - l_p\psi - z_{ip})l_p\} = 0 \quad (11)$$

The rolling motion of sprung mass is given by

$$I\ddot{\theta} + \sum_{i=1}^{2}\sum_{p=1}^{2}\{-cs_{ip}(\dot{z} - b_i\dot{\theta} - l_p\dot{\psi} - \dot{z}_{ip})b_i - ks_{ip}(z - b_i\theta - l_p\psi - z_{ip})b_i\} = 0 \quad (12)$$

The front and rear wheel vertical motion (bounce) can be represented as

$$m_{ip}\ddot{z}_{ip} - cs_{ip}(\dot{z} - b_i\dot{\theta} - l_p - \dot{z}_{ip}) - ks_{ip}(z - b_i\theta - l_p - z_{ip})$$
$$+ cu_{ip}(\dot{z}_{ip} - \dot{h}_{ip} - \dot{v}_{ip}) + ku_{ip}(z_{ip} - h_{ip} - v_{ip}) = 0 \tag{13}$$
$$i = 1,2; \quad p = 1,2$$

The governing differential equation of motion of the box-girder bridge can be expressed as

$$[m_b]\{\ddot{\delta}\} + [c_b]\{\dot{\delta}\} + [k_b]\{\delta\} - \sum_{i=1}^{2}\sum_{i=1}^{2}\{cu_{ip}(\dot{z}_{ip} - \dot{h}_{ip} - \dot{v}_{ip}) + ku_{ip}(z_{ip} - h_{ip} - v_{ip})\}$$
$$+\left(m_s g + \sum_{i=1}^{2}\sum_{p=1}^{2} m_{ip} g\right) + \left(\frac{m_s v^2}{R} + \sum_{i=1}^{2}\sum_{p=1}^{2}\frac{m_{ip}v^2}{R_i'}\right) = 0 \tag{14}$$

The weight of the vehicle and centrifugal forces will also act at appropriate location in addition to the damping and spring forces from vehicle as incorporated in Eq. (14).

Here, $b_1 = a_3 s_2, b_2 = a_4 s_2, l_1 = a_1 s_1, l_2 = a_2 s_1$ and b_2, l_2 are negative quantities. v_{ip} are the bridge displacements under front / rear wheels at any arbitrary time *t*. h_{ip} represents the random input of deck profile under the front / rear wheels and $\dot{h}_{ip}$ are the time derivatives of the random input of deck profile. The suspension stiffness and damping of the vehicle are denoted by ks_{ip} and cs_{ip}. Similarly, the tyre stiffness and damping are denoted by ks_{ip} and cu_{ip}. The unsprung mass is denoted by m_{ip}, which corresponds to tyre mass and m_s represents the sprung mass. The moment of inertia for pitch and roll of the vehicle are designated by J and I, while $[m_b], [c_b], [k_b]$ represents the bridge mass, damping and stiffness matrices respectively and g is the acceleration due to gravity. R is the radius of curvature with respect to the center of gravity of vehicle and R_i' is the corresponding radius of curvature with respect to the right and left wheel.

The set of Eqs. (10) to (14) can be expressed in matrix form amenable to its solution by a suitable numerical scheme as

$$[M]\{\ddot{\chi}\} + [C]\{\dot{\chi}\} + [K]\{\chi\} = \{P\} \tag{15}$$

where $[M]$, $[C]$ and $[K]$ are the global mass, damping and stiffness matrix respectively obtained after assembly and applying boundary conditions. The damping matrix has been taken as Rayleigh's damping matrix (Meirovitch 1986). The response vector $\{\chi\}$ includes the vehicles sprung mass heave, pitch and roll degrees of freedom, unsprung mass vertical bounce and also displacement coordinates defined at the nodal points of the curved bridge. The vector $\{P\}$ represents the generalized force vector which is dependent on pavement roughness, its derivative, moving vehicle mass and centrifugal force due to curvature effect. Newmark-β scheme (average acceleration) with predictor-corrector algorithm (Owen and Hinton 1980) has been used for the evaluation of dynamic response of the bridge due to vehicle-induced vibration. While solving the coupled bridge vehicle system, it is important to examine that any of the tyres does not lose contact with the bridge deck. The tyres of the vehicle always remain in contact with the bridge deck for the range of velocities to be considered such that the interaction force is never less than zero.

2.3 Simulation of deck roughness as input to vehicles

In general, the bridge pavement elevation measured with respect to flat datum at a distance x from the reference station can be represented by

$$h(x) = h_m(x) + h_r(x) \tag{16}$$

where $h_m(x)$ is a deterministic function describing the mean bridge surface profile and $h_r(x)$ is a zero mean random process taken as Gaussian. Discrete form of roughness that includes joint between approach slab and bridge abutment, bump, potholes, construction joint etc can be modeled as a deterministic function bounded in a small interval (Pesterev *et al.* 2002) and be incorporated in the mean roughness profile whenever necessary. The effect of discrete roughness on the dynamic response of bridge is to momentarily increase the contact force between tyre and road surface, thereby increasing dynamic amplification factor (Pesterev *et al.* 2005). In well maintained, bridge such defects will not cause any appreciable increase in the response. In general, the response of such discrete roughness will be transient in nature and its effect on the calculation of fatigue life has been ignored in the present investigation.

The mean surface profile in the present analysis has been taken as flat surface so that $h_m(x) = 0$. The zero mean random process has been modeled by power spectral density function. In time domain analysis, the random road surface roughness $h_r(x)$ of the bridge can be simulated from power spectral density function in the form of a series proposed by Shinozuka (1971) as

$$h(x) = \sum_{k=1}^{N} \alpha_k \cos(2\pi\Omega_k x + \phi_k) \tag{17}$$

where α_k is the amplitude of the cosine wave, Ω_k, is the spatial frequency within the interval $[\Omega_l, \Omega_u]$ in which power spectral density function is defined, φ_k, the random phase angle with uniform probability distribution in the interval $[0, 2\pi]$. x is the global coordinate measured left end of the bridge and N is the total number of terms used to built up the road surface roughness. The value of N depends on the velocity of the vehicle (hence the total time taken to cross the bridge) and size of the time increment chosen for the analysis of the dynamic response (N = Total time/Δt). The parameters α_k and Ω_k are computed as

$$\alpha_k^2 = 4S_r(\Omega_k)\Delta\Omega \tag{18}$$

$$\Omega_k = \Omega_l + (k - 1/2)\Delta\Omega \tag{19}$$

$$\Delta\Omega = (\Omega_u - \Omega_l)/N \tag{20}$$

where $S_r(\Omega_k)$ is the PSD function (m^3/cycle), Ω_l and Ω_u are the lower and upper cut-off spatial frequencies (cycle/m), respectively.

The PSD function $S_r(\Omega_k)$ is expressed in terms of the spatial frequency of the road surface roughness Ω_k (in cycle/m). The following form of PSD of deck roughness suggested by Hwang and Nowak (1991) has been used as the dynamic input to the moving vehicles.

$$S_r(\Omega_k) = \begin{cases} \alpha_s \Omega_k^{-\beta_r}, & \text{for} \quad \Omega_l < \Omega_k < \Omega_u \\ 0 & \textit{else where} \end{cases} \tag{21}$$

Table 1 Road surface classification

Road surface condition	α_s (m^3/(m/cycle))
Very good	$\alpha_s \le 0.24 \times 10^{-6}$
Good	$0.24 \times 10^{-6} \le \alpha_s \le 1.0 \times 10^{-6}$
Average	$1.0 \times 10^{-6} \le \alpha_s \le 4.0 \times 10^{-6}$
Poor	$4.0 \times 10^{-6} \le \alpha_s \le 16.0 \times 10^{-6}$
Very Poor	$\alpha_s > 16.0 \times 10^{-6}$

where the parameter α_s is a spectral roughness coefficient in m^2/(m/cycle) and the spectral exponent β_r is taken to be 1.94. The temporal frequency ω (rad/sec) can be related to spatial frequency of the surface Ω (rad/m) roughness by the following equation

$$\omega = \Omega V \tag{22}$$

in which the V is the vehicle forward velocity. The road surface condition may be classified in to five classes according to ISO specification in terms of coefficient α_s as shown in the Table 1.

3. Damage accumulation and fatigue life

The fatigue behavior is determined experimentally from tests in which a load or deflection is controlled and varied in simple periodic manner until failure. A typical experimental investigation of constant amplitude fatigue for a specimen of given configuration and material involves a large number of tests. The test results are usually presented in the form of S-N curve which is expressed by the relation (Lutes and Sarkani 1997)

$$N_f = KS_r^{-m} \tag{23}$$

in which K and m are the positive material constants whose values depend on both materials and geometry of the specimen; S_r is the stress range and N_f is the number of cycles to failure denoted. The fatigue life of a component is affected by the mean stress and stress range. In conducting the fatigue damage evaluation using mean stress, the failure behaviour in terms of S-N curve needs to be determined using Goodman correction formula (Lutes and Sarkani 1997). In the present study, however, the stress range will be considered in the evaluation fatigue life.

In real situation, a vehicle passing over a bridge induces dynamic load as a result of the vehicle oscillation. These load time histories are much more complicated compared to periodic loadings used in laboratory fatigue testing because of the random nature of the vehicle excitation caused by pavement roughness. The load-time history is generally dominated by one large cycle equal to the peak live load produced by the vehicle. Dynamic effects generate additional small cycles superimposed on the large cycle. In order to assess the fatigue damage caused by the passage of vehicle, it is necessary to account for both the large dominant cycle and the small-superimposed cycles. The basic problem of fatigue analysis is to use appropriately the S-N curve data from the periodic tests to predict fatigue life of an element or assembly, which is subjected to a service load having a complicated time history. In case of random load history, the above equation cannot be used without additional information. The effect of variable-amplitude loading (i.e., random load or irregular) on fatigue performance is normally accounted for with cumulative damage rules. Typically, these rules attempt to relate fatigue behavior under a complex loading history to the known behavior under constant amplitude loading. The linear damage accumulation hypothesis, called “Palmgren-Miner” hypothesis (Lutes and Sarkani 1997) has been used in the present study. The cumulative damage accumulation under variable-amplitude loading is given by

$$D(t) = \sum_{j=1}^{n_b} \Delta D_j = \sum_{j=1}^{n_b} \frac{n_j}{N_j} \tag{24}$$

in which ΔD_j is the incremental damage, n_j is the number of stress cycles at stress range level Sr_j and N_j is the number of cycles at constant stress range level Sr_j from (S-N curve) to cause failure, n_b is the number of stress range blocks in the histogram. The fatigue life T is then calculated as $T = 1/D(t)$. The contribution of small stress cycles below endurance limit in damage summation has been ignored.

Fatigue predictions can follow several approaches, differing in the level of stress and strain analysis used. Moving vehicle induced vibrations of curved box-girder bridge structures produce fluctuating stresses that lead to damage accumulation. Fatigue analysis from vehicle induced stress in a bridge has been carried out in two ways. In the first approach, traditional cycle counting procedures in the time domain has been adopted. The second approach is based on frequency domain criteria in a probabilistic environment, where the spectral density function of the stress is used to determine fatigue life. Time domain analysis of random stress history by cycle counting is computationally expensive. It is necessary to simulate long stress histories and to process each stress range individually to estimate the fatigue damage accumulation. In frequency domain analysis, a power spectral density function of the stresses is used to calculate the probability distribution of the stress peaks. The method used in the frequency domain for the estimation of the fatigue life is Rayleigh’s approximate method, which is applicable for a narrow band Gaussian random process. It provides a rapid estimate of fatigue life that can be compared with the cycle counting method applied on the stress time history.

3.1 Cycle counting method

The cycle counting method has been regarded as a procedure to transform a loading time history into a set of cycles. Fryba (1996) discussed different counting methods for the classification of random time history. In the present paper, Rainflow Counting method (RFCM) has been used in the time domain cycle counting method to identify cycle range. This method establishes one to one correspondence between local maximum and minima of the stress time history. It is observed that in RFCM, small cycles are interruptions of the larger cycles. In this way, the method identifies both slowly varying large amplitude cycles and more rapid small reversals on the top or bottom of these cycles. The sequence of operations followed in RFCM method has been illustrated in Fig. 3.

3.2 Spectral method

In frequency domain method, knowledge of frequency response function and power spectral density of the excitation must be known to obtain the power spectral density of response. For a

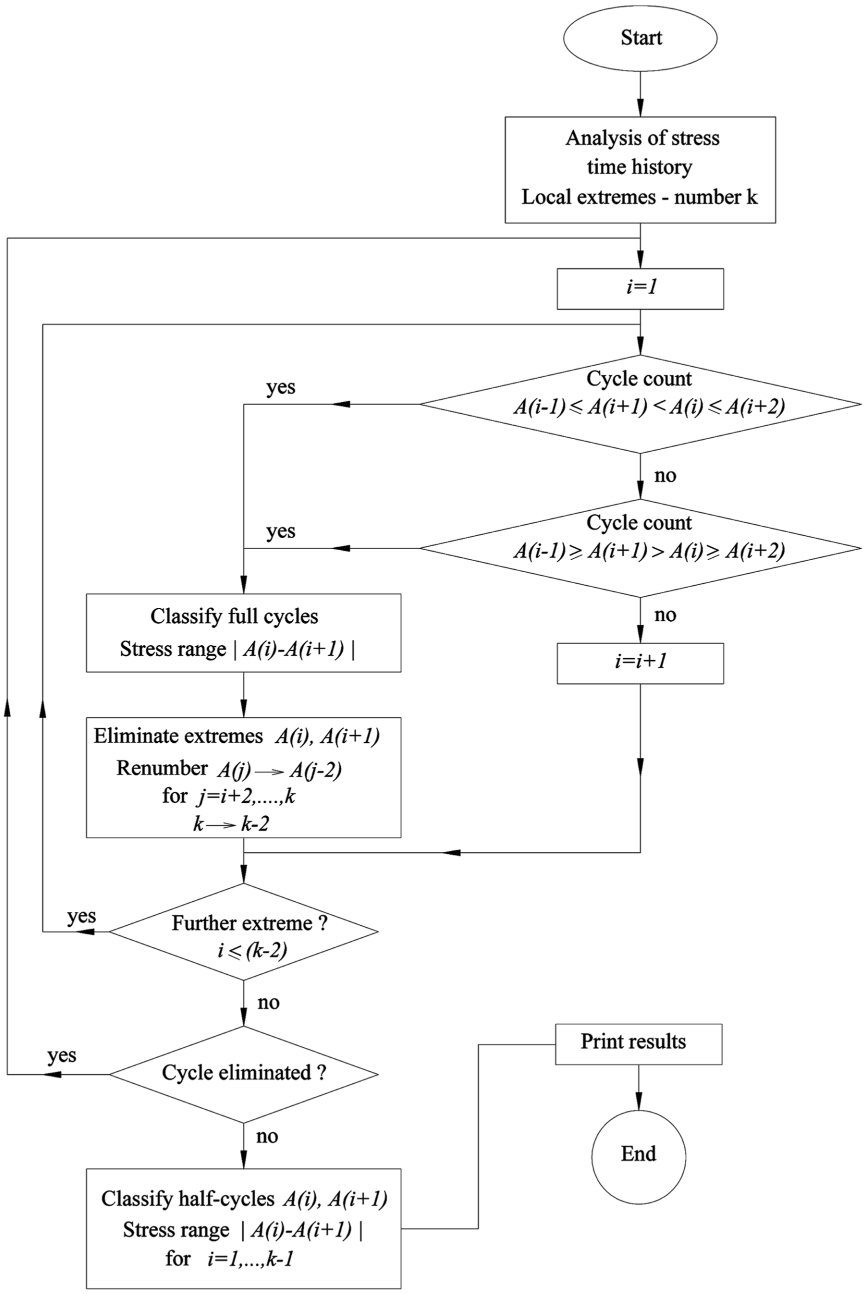

Fig. 3 Flow diagram for the Rain flow counting method [$A(i)$ is the stress at i^{th} time step]

linear time invariant system like the one being presented here, the finite Fourier transform of the force $\{F(\omega)\}$ and response $\{X(\omega)\}$ are related by

$$\{X(\omega)\} = [H(\omega)]\{F(\omega)\} \tag{25}$$

where $[H(\omega)]$ is the complex frequency response function of the system, which is given by

$$[H(\omega)] = [[K] - \omega^2[M]] + i\omega[C]^{-1} \tag{26}$$

The PSD of stress as a function of temporal frequency ω can be defined as

$$[S_{XX}(\omega)] = E[\{X(\omega)\}\{X^*(\omega)\}] = [H(\omega)]^T[S_{FF}(\omega)][H^*(\omega)] \tag{27}$$

in which $[S_{XX}(\omega)]$ is the cross spectral density matrix of the response and $[S_{FF}(\omega)]$ is the cross spectral density matrix of excitation which depends on power spectral density of road roughness selected in the study. It may be noted that no statistical correlation exists between the static vehicle weight and pavement roughness.

In frequency domain, fatigue of structures is estimated based on the statistical properties. The stress PSD functions are usually obtained after solving the equations of motions in frequency domain. To analyse the structural behavior with respect to fatigue, the response must be expressed in terms of stresses.

$$S(x,t) = \bar{S}(x) + s(x,t) \tag{28}$$

where $\bar{S}$ is the mean stress, s is the zero mean fluctuating stress at location x. The mean static stress $\bar{S}$ can be easily derived from the application of the mean static force. Furthermore, assuming that the ratio between the fluctuating and the mean value of stress is equal to the ratio between the fluctuating and the mean value of displacement (Repetto and Solari 2001), the power spectral density of the stress at location x_1 can be derived as

$$S_\sigma(x_1,\omega) = \left[\frac{\bar{S}^2(x_1)}{\bar{X}^2(x_1)}\right] S_{XX}(x_1,\omega) \tag{29}$$

where

$$\{\bar{X}\} = [K]^{-1}\{\bar{F}\} \tag{30}$$

$\{\bar{F}\}$ is nodal load vector for mean force and $S_\sigma(x_1,\omega)$ is power spectral density of stress at location x_1 as function of circular frequency.

3.2.1 Rayleighs approximation

In Rayleigh approximation method, the stress ranges are assumed to have Rayleigh distribution. In particular, each stress range is taken to be twice the random amplitude of the process and for a Gaussian process, this amplitude has a Rayleigh's probability distribution.

Let the k^{th} moment of the spectral density is defined as (Lutes and Sarkani 1997)

$$\lambda_k = \int_0^\infty \omega^k S_\sigma(x_1,\omega)\,d\omega \tag{31}$$

where $S_\sigma(x_1,\omega)$ is the spectral density of stress at location x_1 as function of circular frequency ω. Assuming that S-N curve for the materials are defined, the expected fatigue damage accumulation

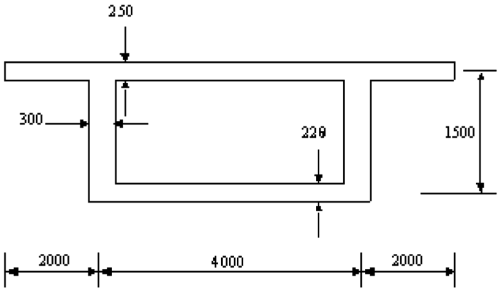

E = 2 e+11 N/m^2
ν = 0.3
G = 7.6923 e+10 N/m^2
ρ = 7840 kg/m^3
I_z = 1.6061 m^4
J = 3.2593 m^4
J_I = 0.79304 m^6
J_{II} = 1.01304 m^6
J_d = 0.00563 m^2
μ_t = 0.365
A = 3.7050 m^2

Fig. 4 Geometry (mm) and properties of box girder bridge

rate can be expressed as (Lutes and Sarkani 1997)

$$E[D(t)]_{t=T} = \frac{K^{-1}2^{3m/2}\lambda_0^{(m-1)/2}\lambda_2^{1/2}\Gamma\left(1+\frac{m}{2}\right)}{2\pi} \tag{32}$$

where λ_0 and λ_2 can be obtained on substitution of $k = 0$ and $k = 2$ respectively in Eq. (31). $\Gamma(.)$ denotes Gamma function.

4. Results and discussion

A simply supported single cell curved box girder bridge (Fig. 4) as considered by Kermani (1993) has been chosen in the present study to obtain the dynamic response due to moving vehicles from which the fatigue life has been estimated. The span of the simply supported bridge is 30 m with a radius of curvature of 150 m and the bridge has diaphragms at supports. The mass density, modulus of elasticity and Poisson's ratio of the material are 7840 kg/m^3, 2×10^{11} N/m^2 and 0.3 respectively.

The first five natural frequencies of the bridge have been found as 38.534 rad/sec, 105.080 rad/sec, 139.907 rad/sec, 208.774 rad/sec and 235.465 rad/sec respectively. In numerical solutions of the coupled bridge vehicle equations of motion, a time step equal to 1/50th of first fundamental time period has been adopted from the accuracy point of view. Further, more refined time increments values have also been considered, which did not show any significant changes in the dynamic response of the bridge under study. Thus, considering numerical error due to inappropriate space and time discretizations, the bridge has been discretized using thirty numbers of thin-walled box beam elements and a time step of 3.6×10^{-3} sec is chosen for the analysis. Damping of the bridge has been taken as one percent of the critical for the first and second modes to obtain the proportionality constants in the expression of Rayleigh's damping. It is assumed that the bridge surfaces have the same roughness in the transverse direction.

All the parameters relevant to the heave-pitch-roll 3D model (Fig. 2) of the vehicle have been taken from the work of Henchi *et al.* (1998) and are presented in Table 2.

Table 2 Physical parameters of vehicle referred in Fig. 2

Parameter	Unit	Value
Sprung mass (m_s)	kg	15000
Unsprung mass in front axle (m_{11}, m_{21})	kg	800
Unsprung mass in rear axle (m_{12}, m_{22})	kg	710
Vehicle suspension stiffness (ks_{ip})	N/m	0.399×10^6
Vehicle tyre stiffness	N/m	0.351×10^6
vehicle suspension damping in front axle (cs_{11}, cs_{21})	Ns/m	23210
vehicle suspension damping in rear axle (cs_{12}, cs_{22})	Ns/m	5180
Vehicle tyre damping (cu_{ip})	Ns/m	800
Pitch moment of inertia (J)	kgm^2	154.536
Roll moment of inertia (I)	kgm^2	449
Position parameter (length wise) a_1, a_2	-	0.35,0.65
Position parameter (breath wise) a_3, a_4	-	0.5,0.5
Vehicle axle spacing (length wise) s_1	m	2.66
Vehicle axle spacing (breath wise) s_2	m	1.5
Height of C.G. of vehicle from deck surface (h_v)	m	1.2

4.1 Road roughness profile

The details of the procedure for generation of random road surface roughness from PSD function have been given in the section 2.3. In this study, the values of spectral roughness coefficient, α_s have been taken as 0.24×10^{-6}, 0.5×10^{-6}, 3.0×10^{-6}, 10.0×10^{-6} and 25.0×10^{-6} m^3/(m/cycle) according to International Organization for Standardization (ISO) specifications for the classes of very good, good, average, poor and very poor roads respectively. Twenty profiles of road roughness have been generated for each type of road using the following parameters:

The lower and upper limits of the spatial frequencies of the road profile are taken as $\Omega_l = 0.01$ cycle/m and $\Omega_u = 3.0$ cycle/m. The cut-off spatial frequencies are chosen in view of the practical

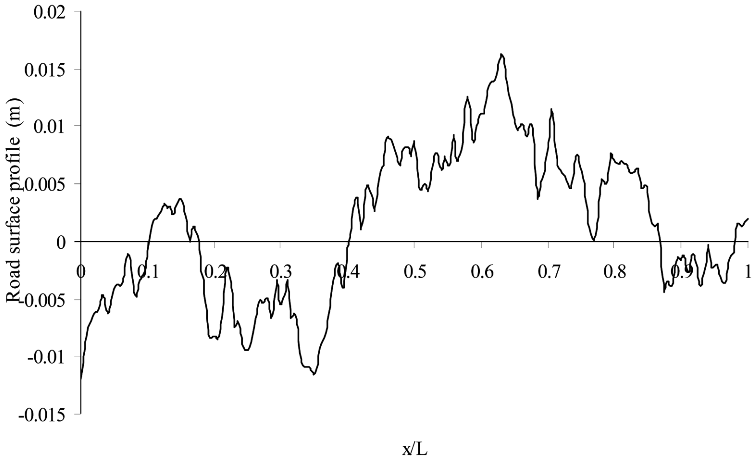

Fig. 5 A typical good road surface profile for a box girder bridge

size of a tyre. A typical vertical surface profile of the bridge deck in 'good road surface category' is shown in Fig. 5. Dynamic responses are evaluated for each of the simulated deck profile corresponding to a particular vehicle velocity.

4.2 Time history of stress

The moving vehicle induces flexural, torsional, warping and distortional warping stresses in thin-walled curved box girder bridge. In the present analysis, for the chosen parameters of the bridge, the magnitudes of flexural stresses dominate over other stresses. Hence for evaluating fatigue life, flexural stresses at mid span have been considered only. Some typical time histories of stress for the bridge are shown in Figs. 6-8. The abscissa in those stress histories is the distance measured from the left end of the bridge to the front axle of the vehicle. The time histories have been obtained for various road surface conditions, varying vehicle speeds and vehicle weight to examine their influence on the fatigue life of the curved bridge.

Slow and fast moving vehicles are covered in the study adopting operating speed range of 5 m/sec (17.8 km/h) to 20 m/sec (71.4 km/h). Fig. 6 shows the flexural stress at mid span in good road surface (Roughness constant $\alpha_s = 0.5 \times 10^{-6}$ m^3/(m/cycle)) condition for different vehicle forward

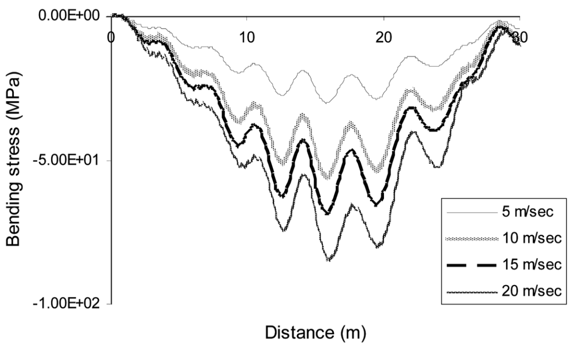

Fig. 6 Flexural stress histories at mid span for different vehicle forward velocities (pavement roughness $\alpha_s = 0.5 \times 10^{-6}$ m^3/(m/cycle), sprung mass (m_s) = 15000 kg)

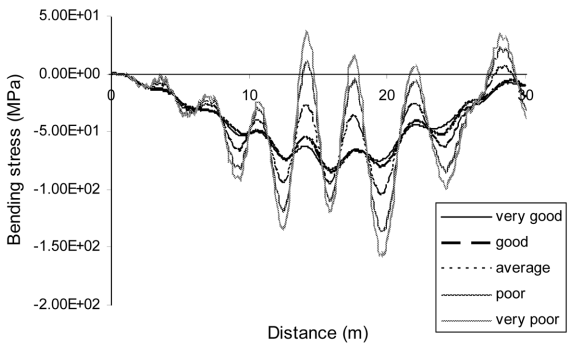

Fig. 7 Flexural stress histories at mid span for different surface category (vehicle velocity = 20 m/sec, sprung mass (m_s) = 15000 kg)

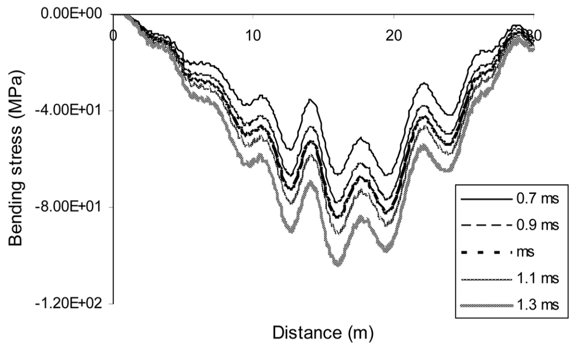

Fig. 8 Flexural stress histories at mid span for different vehicle sprung mass (vehicle velocity = 20 m/sec; Pavement roughness $\alpha_s = 0.5 \times 10^{-6}$ m^3/(m/cycle), sprung mass (m_s) = 15000 kg)

velocities. Fig. 7 and Fig. 8 show the flexural stress at the same location for different road conditions and for different vehicle mass corresponding to constant vehicular velocity of 20 m/sec. The stress time histories exhibit fluctuating components composing of small cycles caused by the dynamic tyre forces generated due to random road roughness, which seems to be superimposed over large cycles caused due to static weight. The peak magnitude is seen to occur when the centre of gravity of vehicle is close to the center of the span, the magnitude of peak being greater for higher velocity, deteriorated road surface condition and increased vehicle weight.

4.3 Stress range histogram

The stress range histogram is needed for the calculation of fatigue life of the bridge. Corresponding to the flexural stress samples at mid span of the bridge obtained by numerical simulation, the stress histogram is prepared after synthesizing the time history by Rain flow counting method. It may be noted that the flexural stresses have been calculated considering the passage of single vehicle over the bridge. Assuming uniform traffic for all the days in a year, number of cycles obtained by Rainflow analysis is simply converted into the annual cycles by using a constant multiplier (Average daily traffic × 365). The flow rates of vehicles over the bridge have been taken as 5×10^5 vehicles annually. Fig. 9 shows a typical stress range vs. frequency (number of cycles/year) histogram with different vehicle forward velocity ranging from 5 m/sec to 20 m/sec in good pavement condition (α_s =0.5 × 10^{-6} m^3/(m/cycle), sprung mass (m_s) = 15000 kg). It is found that the bridge is subjected to maximum 5×10^7 cycles/year in the stress range of 10 MPa-20 MPa (mean stress 15 MPa) in the operating vehicle speed of 5 m/sec to 20 m/sec. In the higher stress range, the numbers of stress cycles experienced by the bridge seem to decline. Fig. 10 presents the stress range vs. frequency histogram obtained for the stress histories corresponding to three different categories of the pavement such as good, average and poor. The vehicle speed considered is 20 m/sec. It reveals from the histogram that the maximum number of stress cycle generated annually corresponds to approximately 4×10^7 cycles/year in the stress range 10 MPa-20 Mpa for the good condition of the bridge deck. The histogram reveals that the number of stress cycles in higher stress

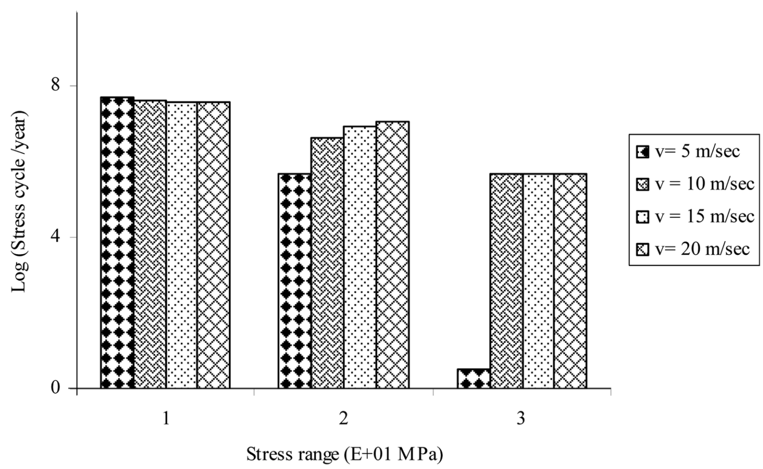

Fig. 9 Stress ranges versus Frequency (cycles/year) Histogram for different vehicle velocity (pavement roughness α_s = 0.5 × 10^{-6} m^3/(m/cycle, sprung mass (m_s) = 15000 kg)

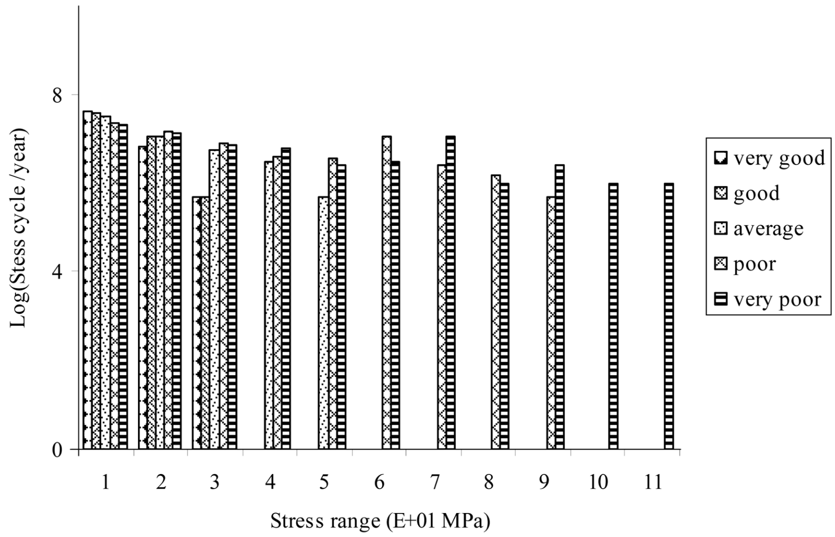

Fig. 10 Stress ranges versus Frequency (cycles/year) Histogram for various surface condition of the deck (vehicle velocity = 20 m/sec, sprung mass (m_s) = 15000 kg)

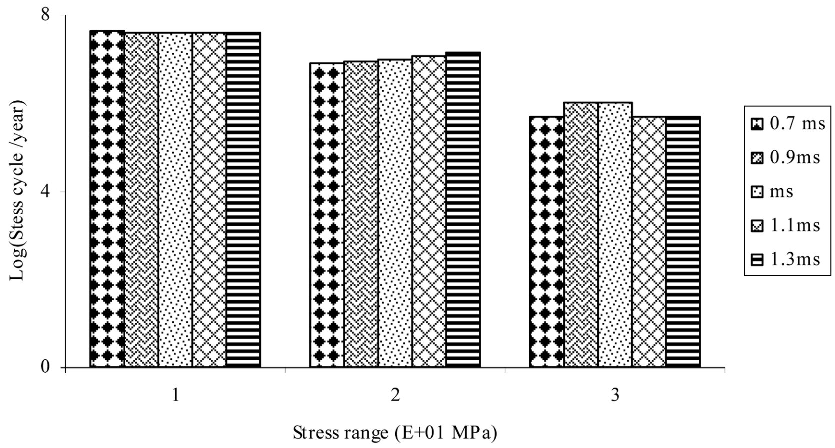

Fig. 11 Stress ranges versus Frequency (cycles/year) Histogram for different vehicle mass (vehicle velocity = 20 m/sec; Pavement roughness $\alpha_s = 0.5 \times 10^{-6}$ m^3/(m/cycle), sprung mass (m_s) = 15000 kg)

range, although very small, is associated with the poor surface condition of the pavement. The number of stress cycles in significant stress range does not reflect much variation due to change of vehicle sprung mass within ±30% limit. This is evident in Fig. 11 which depicts the stress cycle change due to change in vehicle mass when speed is considered as 20 m/sec and pavement roughness (typical of good condition) as $\alpha_s = 0.5 \times 10^{-6}$ m^3/(m/cycle).

4.4 Power spectral density of stress

The power spectral density of stress is necessary for the calculation of spectral moments, which is required to be used for the evaluation fatigue life using Rayleigh's methods. To illustrate the nature

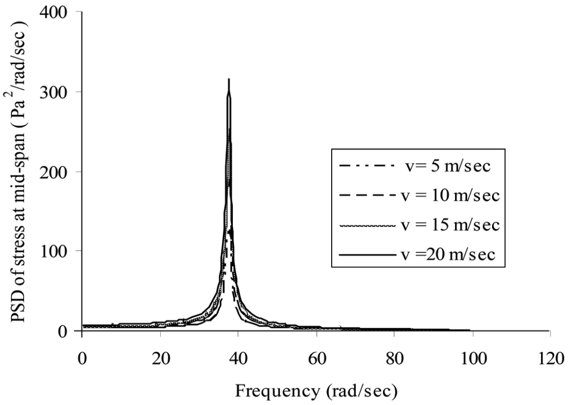

Fig. 12 PSD of flexural stress at mid span for different vehicle velocity (pavement roughness $\alpha_s = 0.5 \times 10^{-6}$ m^3/(m/cycle), sprung mass (m_s) = 15000 kg)

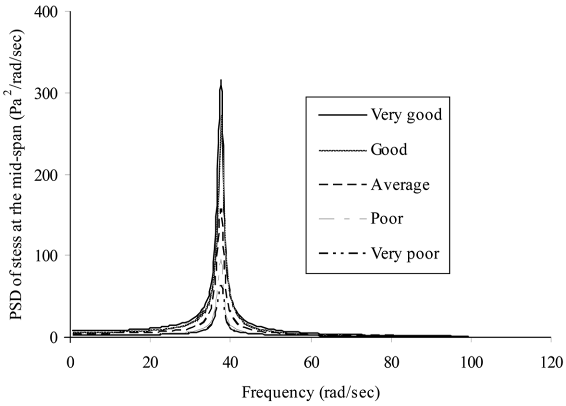

Fig. 13 PSD of flexural stress at mid span for different road surface (vehicle velocity = 20 m/sec, sprung mass (m_s) = 15000 kg)

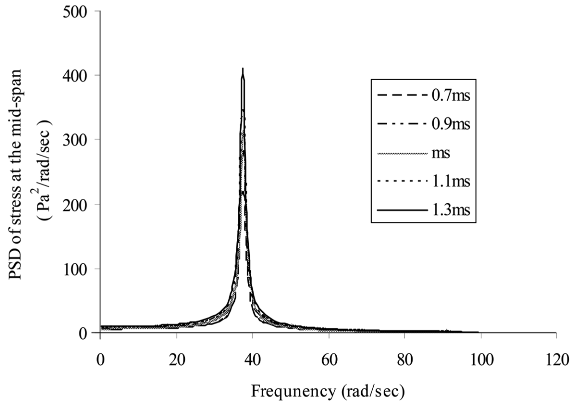

Fig. 14 PSD of flexural stress at mid span for different vehicle mass (vehicle velocity = 20 m/sec; Pavement roughness $\alpha_s = 0.5 \times 10^{-6}$ m^3/(m/cycle), sprung mass (m_s) = 15000 kg)

of the power spectral density of stress, the spectral curve of stresses for of the box-girder bridge have been plotted. Figs. 12, 13 and 14 show the effect of vehicle forward velocity, road roughness and vehicle mass on PSD of stress at the mid-span of box-girder bridge. Results show that all the peaks occur at the fundamental natural frequency of the bridge and has narrow band width centered about the fundamental frequency.

The nature of the PSD curves shows that stresses induced by moving vehicle is the realization of narrow band random process, which justifies the applicability of the Rayleigh's expression for the evaluation of fatigue life. The magnitude of peak for spectral density of stresses increases with the increase of vehicle velocity, road roughness and vehicle mass, which indicates the increase of variance of the flexural stresses.

4.5 Effect of different parameters on the fatigue life

This section examines the effect of some of the important factors, which are believed to influence

Table 3 Influence of S-N curve constant '*K'* (AASHTO-LRFD Fatigue Categories) on fatigue life

Detailed category (Lutes and Sarkani (1997)	Fatigue constant (K) (10^8)	Fatigue life(T) years	
		Spectral method	Cycle counting method
A	250.0	180.668	173.611
B	120.0	86.720	83.333
B'	61.0	44.083	42.361
C	44.0	31.797	30.555
C'	44.0	31.797	30.555
D	22.0	15.898	15.277
E	11.0	7.949	7.638
E'	3.9	2.818	2.708

Pavement roughness $\alpha_s = 0.5 \times 10^{-6}$ m^3/(m/cycle), vehicle speed = 20 m/sec; sprung mass (m_s) = 15000 kg

the fatigue life of the bridge. Fatigue life of the curved thin walled box girder bridge section has been evaluated both by time domain cycle counting analysis and spectral analysis using Rayleigh's approximation.

4.5.1 Effect of S-N curve constants on fatigue life

The constants m and K that are used in the computation of fatigue life of the structure play a very significant role. In calculation of fatigue life, the evaluation of material constants from S-N curve test data is a perquisite. It is difficult to choose the constants m and K without obtaining data of the fatigue test conducted on the specimen. The S-N curves for steel specimen have been presented in AASHTO-LRFD bridge specification (1998) for eight categories of weld details. These fatigue constants K of S-N curve for the steel specimens were used by Chung (2004) for fatigue reliability analysis of steel bridges. The same constants have been used in the present study (Table 3) to examine the fatigue life of a horizontally curved steel bridges. Detailed categories are listed in Table 3 which range from A to E' in order of decreasing fatigue strength. In the present example, the box section is assumed to have continuous welded longitudinal joints and hence it falls to the category B (Chen and Duan 1999). However, various defects in welding, improper sizes or discontinuity and occasional strengthening of section during repairing may lead to weaker or stronger details than the originally designed structure and therefore it is necessary to know how the bridge fatigue life is influenced by such construction defects or strengthening. The results are presented in Table 3 along with detailed categories. The vehicle velocity of 20 m/sec and a good road surface condition (α_s = 0.5×10^{-6} m^3/(m/cycle)) have been assumed. As expected, the predicted fatigue life has been observed to decrease systematically with weaker details. The results obtained by two approaches are sufficiently closer.

4.5.2 Effect of vehicle forward velocity on fatigue life

Table 4 shows the variation of fatigue life due to the variation of vehicle velocity. The fatigue life of the bridge has been computed for good road surface condition with velocity of the vehicle varying from 5 m/sec to 20 m/sec. The effect of increase of speed of the vehicle over the bridge increases the dynamic deflection as well as the peak flexural stress. This leads to the increase of the stress range as well. Higher magnitude of the stress range is expected to reduce the number of cycles to failure. This would result in the increase of cumulative damage index and reduction of

Table 4 Influence of vehicle speed on fatigue life

Vehicle forward velocity m/sec	Fatigue life(T) years	
	Spectral method	Cycle counting method
5	307.272	300.963
10	274.287	267.379
15	210.232	204.918
20	180.668	173.611

Pavement roughness $\alpha_s = 0.5 \times 10^{-6}$ m^3/(m/cycle), sprung mass (m_s) =15000 kg

Table 5 Influence of pavement surface condition on fatigue life

Surface condition	Fatigue life(T) years	
	Spectral method	Cycle counting method
Very Good	241.402	232.558
Good	180.668	173.611
Average	51.684	47.528
Poor	9.598	7.446
Very Poor	4.479	3.656

Vehicle speed =20 m/sec; Sprung mass=15000 kg

fatigue life. A decrease in fatigue life of the girder has been observed corresponding to high-speed vehicular movement along the bridge as shown in Table 4. Further, it is observed that both the methods adopted in the estimation of fatigue life closely agree with each other with Rayleigh's approach being slightly conservative.

4.5.3 Effect of pavement roughness on fatigue life

The surface characteristics play an important role on the dynamic excitation transmitted to the bridge by the moving vehicle. Five categories of surface characteristics have been considered based on the spectral roughness coefficient and classified as very good, good, average, poor and very poor. The effect of any discrete form of roughness such as bump at the approach, construction joints etc. have not been taken into account. The fatigue life corresponding to different response parameters for different categories of road surface have been presented in Table 5. The vehicle velocity has been assumed as 20 m/sec. The fatigue life decreases with the increase in surface roughness. Higher amplitude of tyre force imposed on the pavement due to increased pavement roughness coefficient causes a high value of stress ranges in the bridge girder at the critical sections. The fatigue life reduces irrespective of the vehicle speed for degraded pavement condition. When computed by two methods, Rayleigh's method is again found to yield higher estimate of fatigue life.

4.5.4 Effect of sprung mass on fatigue life

In case of emergency and from strategic point of view, special permits are issued to allow extra heavy loads to pass over the bridge. Therefore, it is necessary to examine the fatigue life of the bridge at increased vehicle weight. The numerical experiment is performed by decreasing and increasing the weight of the vehicle (up to maximum 30%). Table 6 shows the effect of increased

Table 6 Influence of vehicle mass on fatigue life

Vehicle mass	Fatigue life(T) years	
	Spectral method	Cycle counting method
0.7 m_s	217.914	210.084
0.9 m_s	191.972	184.501
1.0 m_s	180.668	173.611
1.1 m_s	175.279	169.491
1.3 m_s	161.256	152.439

Pavement roughness $\alpha_s = 0.5 \times 10^{-6}$ m^3/(m/cycle), vehicle speed=20 m/sec; sprung mass (m_s) = 15000 kg

(or decreased) vehicle mass on the fatigue life of the bridge. The surface condition of the pavement is assumed as 'good'. Uniform vehicle velocity of 20 m/sec is considered for the evaluation of effect of sprung mass variation. It is expected that the deflection and flexural stress in the bridge would increase for the increase of vehicle load. This may result in the increase of higher magnitude stress range causing reduction in the number of cycles to failure. It is observed from the result as shown in Table 6 that the fatigue life decreases with the increase of sprung mass. However, it is seen that with maximum 30% increase of vehicle weight in the present case, the decrease of fatigue life is only about 10%, which may be considered as insignificant in practical situation. Such type of quantitative study is also useful to take decision on the restriction of payload of the vehicle plying over the bridge.

5. Conclusions

A systematic approach has been outlined for the calculation of the fatigue life of a horizontally curved thin walled section box girder bridge considering its dynamic interaction with the vehicle. The key feature of the study is the estimate of fatigue life through the solution of bridge vehicle coupled dynamics with the application of linear damage accumulation rule. A computationally efficient thin walled box-beam finite elements has been used to model curved box-girder bridge which takes into account the torsional warping, distortion and distortional warping, being the important features of thin-walled box girders. Both time domain cycle counting and frequency domain spectral method using Rayleigh's approximate theory have been employed. The spectral method uses an analytical expression for the calculation of fatigue life which is simpler in application and requires less computational time compared to cycle counting method in time domain. The comparative study of the fatigue life of the bridge shows that results of the spectral method, although provides conservative estimate are reasonably closer to the estimates in time domain cycle counting method. The parametric study has been conducted to examine the influence of some of the important parameters on fatigue life as well as to ensure proper model behaviour. Some of the major conclusions are given below:

- The fatigue life of the bridge is dependent on the vehicle weight and the speed of the vehicle. The damage accumulation progresses rapidly due to overload of the vehicle and leads to decrease in the fatigue life. The increase of the vehicle speed also decreases the fatigue life. Thus it is important to regulate the vehicle load and speed over the bridge to increase its life safety limit.

- The condition of the bridge pavement is found to be an important parameter affecting the fatigue life of the bridge. The deteriorated bridge pavement decreases the fatigue life of the bridge.
- The S-N curve constant to be used in fatigue life prediction plays an important role. These constants can drastically change the value of fatigue life.

References

AASHTO-LRFD Bridge Design Specifications (1998), American Association of State Highway and Transportation Officials, Washington, D.C.

Agerskov, H. and Nielsen, J.A. (1999), "Fatigue in steel highway bridges under random loading", *J. Struct. Div.,* ASCE, **125**(2), 152-162.

Amzallag, J.P., Gerey, J.P., Robertt, J.L. and Bahuaud, J. (1994), "Standardization of the rain flow counting method for fatigue analysis", *Probabilist. Eng. Mech.*, **16**, 287-293.

Bennantine, J.A., Commer, J.J. and Handrock, J.L. (1990), Fundamentals of Metal Fatigue Analysis, Prentice Hall, Englewood Cliffs, New Jersey.

Bridge Rules (in SI units) (1964), Ministry of Railways, Govt. of India., Revised

BS: 5400: Part 10 (1980), Steel, Concrete and Composite Bridges-Part10: Code of Practice for Fatigue, British Standards Institution.

Chen, W. and Duan, L. (1999), "Bridge Engineering Hand Book", CRC Press, Washington D. C.

Chung, H.Y. (2004), Fatigue Reliability and Optimal Inspection Strategies for Steel Bridges, Ph.D Thesis, The University of Texas, Austin.

Dougall, C.M., Green, M.F. and Shillinglaw, S. (2006), "Bridge fatigue life estimation from field data", *J. Bridge Eng.*, **11**(3), 320-328.

Dowling, N.E. (1972), "Fatigue failure predictions for complicated strain histories", *J. Mater.*, **7**(1), 71-87.

Fryba, L. (1996), *Dynamics of Railway Bridges*, Thomas Telford.

Guide Specifications for Fatigue of Steel Bridges (1989), American Association of State Highway and Transportation Officials (AASHTO), Washington, D.C.

Henchi, K., Fafard, M., Dhatta, G. and Talbot, M. (1998), "An efficient algorithm for dynamic analysis of bridge under moving vehicle using a coupled model and physical components approach", *J. Sound Vib.*, **12**, 663-683.

Huang, D.Z., Wang, T.L. and Shahaway, M. (1993), "Probabilistic fatigue life analysis of highway steel bridges", *J. Comput. Struct.*, **48**(2), 241-248.

Hwang, E.S. and Nowak, A.S. (1991), "Simulation of dynamic load for bridges", *J. Struct. Eng.* ASCE, **117**, 1413-1434.

IRC-22 (1986), Standard Specifications and Code of Road Bridges, Section-VI, Composite Construction.

Kermani., B. and Waldron, P. (1993), "Analysis of continuous box girder bridges including the effects of distortion", *Comput. Struct.,* **47**, 427-440.

Kihl, D.P., Sarkani. S. and Beach, J.E. (1995), "Stochastic fatigue damage accumulation under broadband loadings", *Int. J. Fatigue*, **17**(5), 321-329.

Larsen, C.E. and Lutes, L.D. (1991), "Predicting the fatigue life of offshore structures by the single-moment spectral method", *Probabilist. Eng. Mech.*, **6**(2), 96-108.

Lutes, L.D. and Sarkani, S. (1997), Stochastic Analysis of Structural and Mechanical Vibrations, Prentice Hall, Upper Saddle River, New Jersey.

Lutes, L.D., Corazao, M., Hu, S.J. and Zimmerman, J. (1984), "Stochastic fatigue damage accumulation", *J. Struct. Eng.*, ASCE, **110**(11), 2585-2601.

Meirovitch, L. (1986), Elements of Vibration Analysis, McGraw Hill International edition, Mechanical Engineering Series.

Miner, M.A. (1945), "Cumulative damage in fatigue", *J. Appl. Mech.*, ASME, **67**, 159-164.

Mohammadi, J., Guralnick, S.A. and Polepeddi, R. (1998), "Bridge fatigue life estimation from field data", *Pract. Periodical Struct. Des. Constr.*, ASCE, **3**, 128-133.

Nallasivam, K., Dutta, Anjan and Talukdar, Sudip. (2007), "Dynamic analysis of horizontally curved thin-walled box-girder bridge due to moving vehicle", *Shock Vib.*, **14**, 229-248.

Owen, D.R.J. and Hinton, E. (1980), Finite Elements in Plasticity: Theory and Practice, Pineridge Press Limited, Swansea, U.K.

Paris, P. and Erdogen, F. (1963), "A critical analysis of crack growth propagation laws", *J. Basic Eng.*, ASME, **85**(3), 528-534.

Park, Y., Han, S. and Suh, B. (2005), "Fatigue reliability analysis of steel bridge welding member-fracture mechanics method", *Struct. Eng. Mech.*, **19**(3), 347-359.

Pesterev, A.V., Bergman, L.A. and Tan, C.A. (2002), "Pothole induced contact forces in a simple vehicle model", *J. Sound Vib.*, **256**, 565-572.

Pesterev, A.V., Bergman, L.A., Tan, C.A. and Yang, B. (2005), "Assesing tire forces due to roadway unevenness by the pothole dynamic amplification factor method", *J. Sound Vib.*, **279**, 817-841.

Ravi, G. and Ranganathan, R. (1994), "Fatigue crack reliability of riveted bridge", *Int. J. Struct.*, **14**(2), 103-108.

Repetto, M.P. (2005), "Cycle counting methods for bi-model stationary Gaussian processes", *Probabilist. Eng. Mech.*, **20**, 229-238.

Repetto, M.P. and Solari, G. (2001), "Dynamic along wind fatigue of slender vertical structures", *Eng. Struct.,* **23**, 1622-1633.

Shinozuka, M. (1971), "Simulation of multivariate and multidimensional random processes", *J. Acoust. Soc. Am.*, **49**, 357-367.

Wang, T.L., Liu, M. and Huang, D. (2000), "Truck loading and fatigue damage analysis for girder bridges based on the weight-in-motion data Bridge", *J. Bridge Eng.*, **10**(1), 12-20.

Wirsching, P.H. and Light, M.C. (1980), "Fatigue under wide band random process", *J. Struct. Eng.*, ASCE, **106**(ST7), 1593-1607.

Woo, K.S., Hong, C.H. and Basu, Pt.K. (2004), "J-integral and fatigue life computations in the incremental plasticity analysis of large scale yielding by p-version of F.E.M", *Struct. Eng. Mech.*, **17**(1), 51-68.

Zhang, S.H. and Lyons, L.P.R. (1984), "A thin-walled box beam finite element for curved bridge analysis", *Comput. Struct.*, **18**, 1035-1046.

Zhao, Z., Halder, A. and Breen, F.L. Jr. (1994), "Fatigue reliability evaluation of steel bridges", *J. Struct. Eng.*, ASCE, **120**(5), 1608-1622.